Nanoscale

Accepted Manuscript

This article can be cited before page numbers have been issued, to do this please use: Y. Wang, Y. Zhu, S. Afshar, M. WOO, J. Tang, T. Williams, B. Kong, D. Zhao, H. Wang and C. Selomulya, *Nanoscale*, 2019, DOI: 10.1039/C8NR08418A.

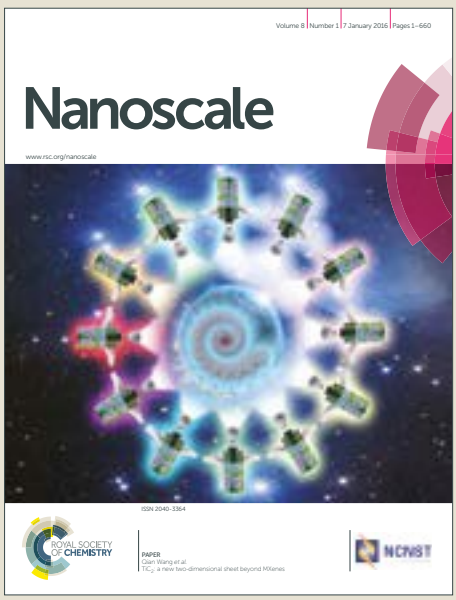

ROYAL SOCIETY OF CHEMISTRY

rsc.li/nanoscale

ROYAL SOCIETY OF CHEMISTRY
View Article Online
DOI: 10.1039/C8NR08418A

Journal Name

COMMUNICATION

One Dimensional CoS_2-MoS_2 Nano-flakes Decorated MoO_2 Sub-micro-wires for synergistically Enhanced Hydrogen Evolution

Received 00th January 20xx,
Accepted 00th January 20xx

DOI: 10.1039/x0xx00000x

www.rsc.org/

Yang Wang, †[a] Yinlong Zhu, †[a] Sepideh Afshar, [a] Meng Wai Woo, [a] Jing Tang,[b] Timothy Williams,[d] Biao Kong,[c] Dongyuan Zhao,*[ac] Huanting Wang,*[a] Cordelia Selomulya,*[a]

CoS_2-MoS_2 nanoflakes decorated MoO_2 (CoMoOS) hybdrid submicro-wires with rich active interfaces were synthesized via sulfuration of $CoMoO_4$. They showed excellent activities in synergistically catalyzing hydrogen evolultion reaction (HER) in basic media by promoting both the water dissociation and hydrogen absorption steps. Thus, the CoMoOS catalysts only needed 123 mV to achieve 10 mA·cm^{-2} with a small Tafel slope in alkaline solutions, and required 1.68 V to obtain the same current density when assembled into an alkaline electrolyser.

Hydrogen (H_2), with the highest gravimetric energy density and zero carbon footprint, is widely considered as a promising energy carrier to fuel our society cleanly and sustainably. H_2 produced by water splitting is highly desirable due to the large quantities of energy harvest without emission of green-house gases and other undesirable side-products.[1-3] Water splitting consists of two half reactions: anodic oxygen revolution reaction (OER) and cathodic hydrogen evolution reaction (HER) which is the actual process to generate H_2.[4, 5] When OER and HER catalysts are assembled into an electrolyser, different electrolytes including acidic, alkaline and neutral media can be used. Compared to a neutral electrolyser, acidic and alkaline ones are efficient enough for commercial use. However, just a few of non-noble metal compounds have been studied as OER electro-catalysts for acidic electrolysers,[6, 7] while most acidic electrolysers in acidic solutions still require noble metal based catalysts such as IrO_2 or RuO_2 as OER electro-catalysts due to the in-stability of earth-abundant transition metal compounds as OER electro-catalysts in a low pH condition.[8, 9] Therefore, alkaline electrolyser will be more economical when assembled by non-noble metal based materials due to the cost-effective and highly active earth–abundant OER electro-catalysts in basic media.[10-17] However, HER kinetics are sluggish in alkaline solutions, almost two orders of magnitude slower than in acidic solutions.[18-20] The sluggish kinetics in basic solutions impede the development of alkaline electrolysers based on non-noble metal electro-catalysts. Therefore, it is necessary to develop highly effective HER catalysts in alkaline solutions based on cheap and earth-abundant elements.[21-28]

As a kind of non-noble metal catalysts, transition metal disulfides such as MoS_2, NiS_2, CoS_2 and FeS_2 always display good performance in acidic solutions.[29-35] For example, MoS_2 has emerged as a highly active noble metal-free HER catalysts in acidic solutions, however, its HER performance in alkaline solutions is inferior to that in acidic media, due to the sluggish water dissociation kinetics.[36] In general, the HER process in alkaline media typical involves two steps: electron-coupled water dissociation to form H_{ad} (the Volmer step) and the concomitant conversion of H_{ad} into molecular H_2 (the Heyrovsky or Tafel step).[37-40] Therefore, promoting the water dissociation process is also crucial to an optimal HER catalyst operating in alkaline media besides tuning suitable hydrogen adsorption free energy. Recent studies have proven that oxides or hydroxides (e.g., NiO, TiO_2, Mn_3O_4, $NiTiO_3$, $Ni(OH)_2$, $Co(OH)_2$ and $NiCo_2O_4$) can effectively facilitate water dissociation.[41-47] Besides, MoO_2 was also demonstrated to have a metallic property and reasonable HER activities.[48] Therefore, various hybrid materials have been developed as efficient HER catalysts in alkaline media owing to the synergistic effect produced by the interfacial interaction between multiple components.[49-52]

Based on the above considerations, we postulated that ultrathin MoS_2-CoS_2 nanoflakes decorated MoO_2 submicro-wires could synergistically facilitate the HER process in alkaline solutions, which followed the design criteria of effective non-noble metal HER catalysts in alkaline solutions: 1) appropriate hydrogen adsorption

[a] Department of Chemical Engineering, Monash University, Clayton, Victoria 3800, Australia
[b] Department of Materials Science and Engineering, Stanford University, Stanford, California, USA
[c] cCollaborative Innovation Center of Chemistry for Energy Materials (iChEM), Department of Chemistry, Laboratory of Advanced Materials, Fudan University, Shanghai 200433, P. R. China
[d] Monash Centre for Electron Microscopy (MCEM), Monash University, Clayton, Victoria 3800, Australia
† Y. Wang and Y. Zhu contributed equally to this work.
Electronic Supplementary Information (ESI) available. See DOI: 10.1039/x0xx00000x

ability of metal disulfieds (MoS_2 and CoS_2) and favourable water-dissociation (MoO_2) during HER by introducing appropriate components; 2) exposing more active sites by nano-size-tuning the active components (nanoflakes) to obtain high electrochemical surface area (ECSA); 3) enhanced charge transfer during electrochemical catalytic process (MoO_2). The obtained MoS_2-CoS_2@MoO_2 (CoMoOS) hybrid shows a high HER performance with a small over-potential of 123 mV to achieve 10 mA·cm^{-2} and a low Tafel slope of 86 mV·dec^{-1} in the alkaline solution.

The morphology of CoMoOS was first examined by scanning electron micron microscopy (SEM) (**Fig. 1a**), the diameter of CoMoOS wires is between 100-400 nm and the surface is much rougher than its $CoMoO_4$ precursor (**Fig. 1a, inset**). This rough surface consists of nano-flakes, according to the low-magnification TEM image (**Fig. 1b, inset**), which can be further confirmed by the HR-TEM image (**Fig. 1b**) in which the lattice fringes with an interplanar spacing of 0.63 and 0.25 nm, correspond to the (002) plane of MoS_2 and the (210) plane of CoS_2, respectively.

The composition of CoMoOS were also determined by XRD patterns (**Fig. 1c**). The characteristic peak at 16.7 corresponds to the (002) plane in MoS_2 (**PDF No. 04-004-5723**) which has a *Molybdenite-2H* phase structure. Another characteristic peak at 30.4 is ascribed to the (011) plane in MoO_2 (**PDF No. 04-007-2356**) with a *Tugarinovite* phase structure. The other obvious peaks at 32.5, 37.8, 42.4, 46.7, 54.5, 64.9, 68.2, 71.4 and 74.5 belong to the (111), (200), (210), (211), (220), (311), (222), (023) and (321) planes, respectively, in CoS_2 (**PDF No. 04-003-1962**) of a *Cattierite* phase structure. Besides, the percentage (mass) of MoO_2, MoS_2 and CoS_2 in CoMoOS were estimated to be 1.6%, 72.5% and 25.9% by XRD quantitative analysis – Rietveld method (**Table s1, ESI**). E_{1g}, $E_{2g}{}^1$ and A_{1g} modes belonging to MoS_2 were also detected in CoMoOS shown in Raman spectra (**Fig. s2, ESI**).

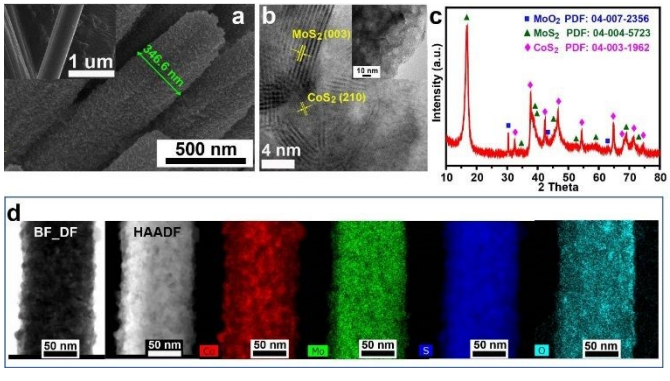

Figure 1. Characterization of the as-prepared CoMoOS micro-meter wires. (**a**) SEM image (inset: SEM image of $CoMoO_4$). (**b**) HTEM image (inset: low magnification). (**c**) XRD patterns. (**d**) STEM images of CoMoOS: Bright Field_ Dark Field (BF_DF) and high-angle annular dark-field (HAADF) STEM images; EDS mapping single element of Co, Mo, S and O in CoMoOS.

In order to identify the distributions of all the elements in CoMoOS, STEM-EDS element mappings are shown in **Fig. 1d**, which shows the uniform distribution of Co, Mo, S and O along the wire, demonstrating that the *in situ* generated CoS_2, MoS_2 and MoO_2 are mixed at the nanoscale, providing many favourable interfaces. Qualitative evidence provided by XPS (**Fig. s3, ESI**) confirmed that the surface of CoMoOS (top few nm) consisted mainly of the metal sulfides (CoS_2 and MoS_2) with minor concentration of oxides being also present, which may result from slight surface oxidation of the sample in air. [53, 54]

The optimal sulfuration condition was obtained by studying the influence of sulfuration temperature and duration, different mass of sulfur as well as using a spacer boat during the sulfuration of $CoMoO_4$ (**Fig. s8**). When $CoMoO_4$ underwent sulfuration at a temperature of 500 °C for 30 minutes by using 1.5 g of sulfur, the obtained CoMoOS showed the best HER performance among all the conditions studied. When a spacer boat between the boats containing sulfur and $CoMoO_4$ was used, the performance was further improved by reducing 26 mV of the overpotential to obtain a current density of 10 mA·cm^{-2}. To better understand the function of the spacer boat, (CFD) model (**Fig. s9**) was applied to describe the effect of spacer boat on the flow of nitrogen as carrier gas in the sulfuration process. CFD calculation result shows that adding a spacer between the boats can lead to a more developed turbulent flow due to the developing reversed flow near to the boats' edges. As a result, a better mixing of sulfur and $CoMoO_4$ can be achieved at higher turbulence caused by the spacer boat.

The electro-catalytic performance of CoMoOS was evaluated by the polarization curves from linear sweep voltammetry (LSV) in 1.0 M KOH electrolyte using copper foam (CF) as the current collector. The LSV curves are obtained at a slow scan rate of 5 mV s^{-1} to minimize the capacitive current. All the potential values presented in this work were *iR*-corrected (aiming to remove the ohmic potential drop) and referenced to the hydrogen electrode (RHE) unless indicated otherwise. For comparison, similar measurements are performed on CoMoOS, MoO_2, MoS_2, CoS_2 and physical mixture of MoO_2/MoS_2/CoS_2. The morphology and XRD patterns of commercial MoO_2, synthesized MoS_2 and CoS_2 are displayed in **Fig. s4.** From **Fig. 2a**, it is obvious to see CoMoOS exhibits a very small onset potential of 65 mV and an low overpotential (η_{10}) of 130 mV to achieve a current density of 10 mA·cm^{-2} while the copper foam (CF) substrate has a negligible activity towards HER in 1.0 M KOH. However, $CoMoO_4$ displays a large overpotential of 214 mV to achieve a current density of 10 mA·cm^{-2}. As for single component of MoS_2 and CoS_2, their η_{10} are 302 mV and 273 mV, respectively, while the η_{10} of MoO_2 is much more than 320 mV. When MoO_2, MoS_2 and CoS_2 were physically mixed together (denote as MoO_2/MoS_2/CoS_2) according to the mass ratio detected by XRD, the overpotential to achieve 10 mA·cm^{-2} is 258 mV which is lower than that of the single components but still much larger than that of CoMoOS, which demonstrates the favourable functions of each component as well as the synergistic

effects of components in the nano-hybrid. To get rid of the effect from the porous substrate, glassy carbon (GC) was also used to test the performance of these catalysts (**Fig. s5, ESI**) and CoMoOS also displayed the best performance among these catalysts.

As an important parameter of electrolysis, Tafel slope describes the over-potential needed to increase the current density by ten-fold, which reflects the kinetics of HER. Compared with $CoMoO_4$ (133 mV·dec^{-1}), CoMoOS has a smaller Tafel slope of 86 mV·dec^{-1} (**Fig. 2b**), demonstrating its fastest kinetics towards HER; while the Tafel slopes of MoO_2, MoS_2, CoS_2 and $MoO_2/MoS_2/CoS_2$ physical mixture are 334, 120, 180 and 135 mV·dec^{-1}. Hence, CoMoOS hybrid possesses the fastest HER kinetics process among all the catalysts reported in this work. According to the mechanism of hydrogen evolution, the HER process consists of two principal steps in alkaline electrolytes. The initial discharge step is called Volmer reaction ($H_2O + e^- \rightarrow H_{ads} + OH^-$) with a high Tafel slope of 120 mV·dec^{-1}. Then, Heyrovsky reaction (the electrochemical desorption step): $H_{ads} + H_2O + e^- \rightarrow H_2 + OH^-$ or Tafel reaction (the recombination step): $H_{ads} + H_{ads} \rightarrow H_2$ happens after Volmer reaction with a relative lower Tafel slope of 40 and 30 mV·dec^{-1}, respectively. The Tafel slope of CoMoOS is 86 mV·dec^{-1} which lies between 40 and 120 mV dec^{-1}, suggesting that a Volmer–Heyrovsky mechanism might be responsible for the HER process in CoMoOS.

The stability of CoMoOS for HER is also excellent with just 106 mV increase after electrolysis at -10 mA·cm^{-2} for 40 h (**Fig. 2c**). The LSV recorded before and after the 40 h of testing at a scan rate of 5 mV·s^{-1} are shown in **Fig. 2d**. Only a minimal loss in activity at a current density of 10 mA cm^{-2} is observed. Therefore, there is a very good agreement between the galvanostatic stability tests, reaffirming that CoMoOS is potentially a very stable catalyst. Regarding the mass loading effect, HER performance can be improved when tripled the mass loading of CoMoOS from 0.8 to 2.4 mg·cm^{-2}. When the mass loading was further increased, the HER performance decreased due to the overloaded catalysts on the limited surface of the copper foam (**Fig. 2d**).

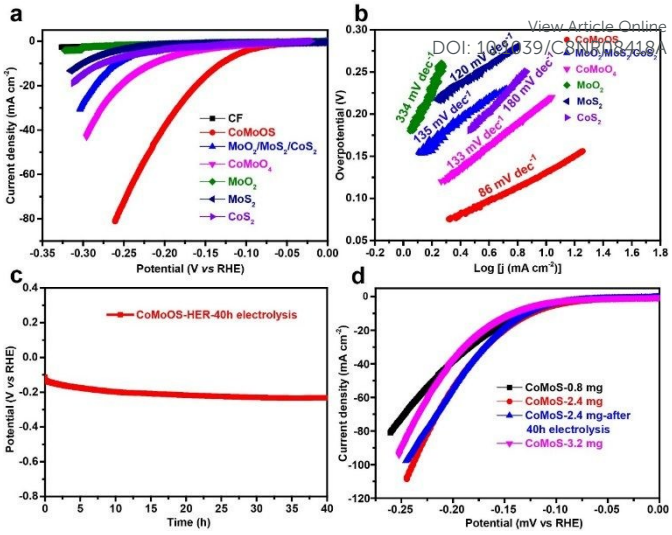

Figure 2. **(a)** Polarization curves, **(b)** Tafel plots of copper foam (CF), CoMoOS, $CoMoO_4$, commercial MoO_2, MoS_2 and CoS_2, $MoO_2/MoS_2/CoS_2$ physical mixture (0.8 mg on CF) in 1.0 M KOH. **(c)** Chronopoteniometric curve of CoMoOS catalyst (2.4 mg on CF) at a current density of -10 mA·cm^{-2} for 40 h and **(d)** Polarization curves of CoMoOS with different mass loading.

The superior HER performance of CoMoOS compared to the $CoMoO_4$ precursor and the single components as well as the $MoO_2/MoS_2/CoS_2$ physical mixture might be due to the following three aspects:

(1) Synergetic effects between different components of CoMoOS. Although MoS_2 and CoS_2 are favourable to hydrogen adsorption during HER, their performance in alkaline solutions is still limited by the sluggish water dissociation step which can be facilitated by transition metal oxides.[36, 46, 55-57] Thus, introducing MoO_2 can improve the HER performance of the whole hybrid by promoting the water dissociation during Volmer step. Besides, the introduction of MoO_2 with metallic properties will also improve the charge transfer of the hybrid according to the reports in previous literature.[58] Therefore, a similar mechanism is proposed here that MoO_2 acts as water dissociation facilitator while CoS_2-MoS_2 together promote the hydrogen absorption during HER process (**Fig. 3a**). Besides, the uniform distribution of Co, Mo, O and S (**Fig. 1d**) indicates intimate interactions among CoS_2, MoS_2 and MoO_2, which leads to a strong electron interactions and enable the surface electronic state to reach a favourable hydrogen absorption free energy for promotion of HER. In addition, the interfaces formed among MoO_2, CoS_2 and MoS_2 might cause doping effects by introducing Co and O into MoS_2 and generate abundant defect sites that would act as catalytically active sites for the HER.[59, 60,61].

(2) One dimensional hierarchical structure with high electrochemical surface area (ECSA) of CoMoOS. The hierarchical structure enable the hybrid have various size of channels and pores for mass transport (**Fig. s1a, b, ESI**). For example, the macropores or channels originated from the interlacing of the one dimensional sub-microwires can facilitate mass (electrolyte or gas products) transfer. Besides, the meso-pores formed by the stacking of CoS_2 and MoS_2 nanoflakes can

provide high ECSA and expose plenty of active sites for HER. ECSA was calculated from the specific capacitance. Normally, specific capacitance for 1 cm^2 of a flat surface is around 20-60 $\mu F \cdot cm^{-2}$ and the average value of 40 $\mu F \cdot cm^{-2}$ is generally used for calculations. The specific capacitance (**Fig. 3d**) can be obtained from geometric current density collected from the rectangular CV plots (**Fig. 3c**) at a certain potential of 0.15 V *vs* RHE. The specific capacitance of CoMoOS is 46.3 $mF \cdot cm^{-2}$ which is larger than that of $CoMoO_4$ (2.7 $mF \cdot cm^{-2}$), MoO_2 (1.5 $mF \cdot cm^{-2}$) and CoS_2 (24.6 $mF \cdot cm^{-2}$), due to the nanosize of the active CoS_2 and MoS_2 nanflakes which can expose more active sites. Although MoS_2 and $MoO_2/MoS_2/CoS_2$ mixture show a higher specific capacitance than that of CoMoOS due to the nanosheet structure of MoS_2 (**Fig. s2b, e, EIS**) with higher surface area, the intrinsic poor conductivity of MoS_2 hinders the charger transfer which decreases the HER performance of both MoS_2 (89.8 $mF \cdot cm^{-2}$) and $MoO_2/MoS_2/CoS_2$ mixture (60.4 $mF \cdot cm^{-2}$). The high specific capacitance of CoMoOS demonstrates that there are a large amount of exposed active sites in CoMoOS for HER. The high ECSA might be derived from the meso-pores (typical plot for meso-pores in **Fig. s1a, EIS**) stacked by MoS_2 and CoS_2 on the surface of MoO_2. The diameter of the pore is around 20-150 nm (**Fig. s1b, ESI**). In contrast, the smooth surface of $CoMoO_4$ (**Fig. 1b, inset**) and bulk MoO_2 (**Fig. s4a, d, ESI**) enable them have very low ECSA, demonstrating the importance of the nano-design of the active components in hybrid.

(3) Low charge transfer resistance. The electrochemical impedance spectroscopy (EIS) was carried out to investigate the HER process of catalysts in this work (**Fig. 3b**). The EIS data of CoMoOS was fitted by equivalent circuit model which showed two semi-circles (**Fig s6, ESI**). The semicircle at high frequency reflected the contact resistance between copper foam and CoMoOS, while the semicircle at middle and low frequency related to the charge transfer on the surface of the catalyst.[62, 63] Charge transfer resistance (R_{ct}) is usually used to assess the kinetics of electrochemical process on the surface of catalysts. The smaller the R_{ct} reflects the faster kinetics thus leads to a larger current density. The results for the elements in circuit are shown in **Table s2**. The CoMoOS displays the smallest diameter of the semicircle shown in the electrochemical impedance diagram (**Fig. 3b**) which represents the smallest charge transfer resistance (~2.1 ohm) during HER process; in contrast the charge transfer resistance of $CoMoO_4$, MoO_2, MoS_2 and CoS_2 and $MoO_2/MoS_2/CoS_2$ mixture are 8.9, 104, 53, 42 and 21 ohm respectively. The favourable charge transfer of CoMoOS is ascribed to its favourable nano-interfaces which boost the charge transfer.

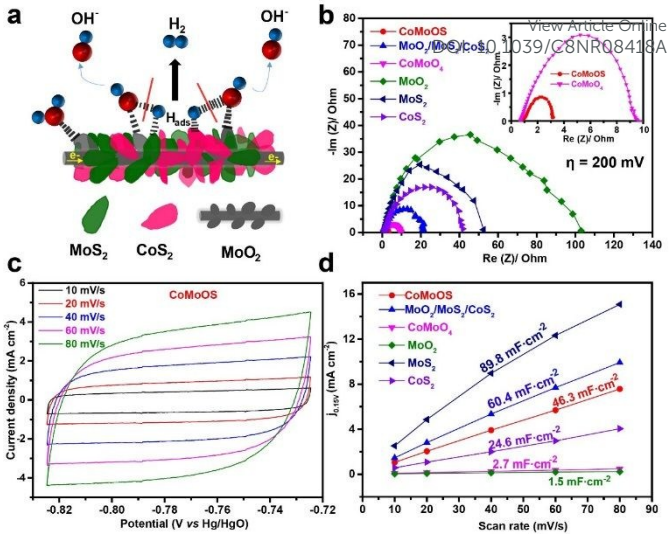

Figure 3. **(a)** Schematic representation of water dissociation, formation of M-Had intermediates, as well as subsequent recombination of two H_{ad} atoms to form H_2 on CoS_2-MoS_2-MoO_2 (CoMoOS) electro-catalyst. **(b)** Nyquist plots at an overpotential of 200 mV for CoMoOS, $CoMoO_4$, MoO_2, MoS_2, CoS_2 and $MoO_2/MoS_2/CoS_2$ physical mixture. (**c**) CV curves of CoMoOS at different scan rate with a potential range of -0.824 ~ -0.724 *vs* Hg/HgO. (**d**) Scan rate dependence of the current densities of CoMoOS, $CoMoO_4$, MoO_2, MoS_2, CoS_2 and $MoO_2/MoS_2/CoS_2$ physical mixture at 0.15 V *vs* RHE.

In addition to the high HER activity in alkaline solutions, CoMoOS also showed high OER performance (**Fig. s7, ESI**) in alkaline media with a small overpoetential of 260 mV to achieve 10 $mA \cdot cm^{-2}$ and a low Tafel slope of 75.2 $mV \cdot dec^{-1}$. To demonstrate the feasibility of using CoMoOS as both cathode and anode for overall water splitting (**Fig. 4a**), only 1.68 V is needed to achieve 10 $mA \cdot cm^{-2}$ while the $MoO_2/MoS_2/CoS_2$ mixture needs 1.74 V to reach 10 $mA \cdot cm^{-2}$. The copper foam substrate shows negligible performance for water splitting. The potential of CoMoOS for water splitting is lower than other catalysts reported recently (**Fig. 4c**). The stability of CoMoOS for overall water splitting is excellent with just 38 mV increase after 24 h electrolysis at a current density of 10 $mA \cdot cm^{-2}$ (**Fig. 4b**). Gas bubbles were observed at both electrodes in **Fig. 4d.**

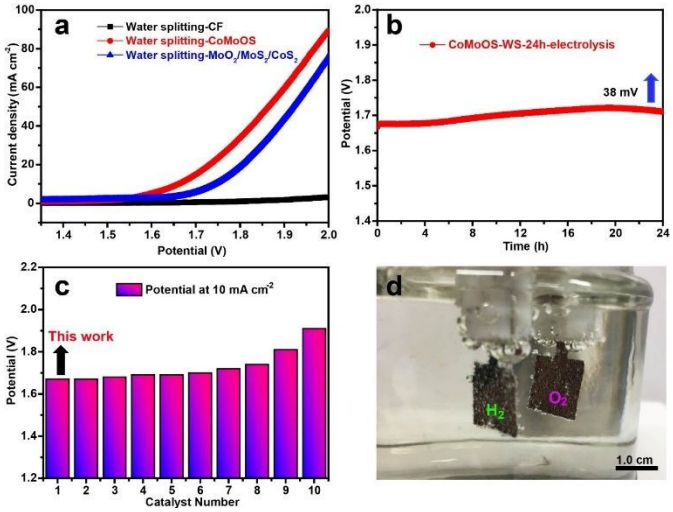

Figure 4. (**a**) Polarization curves of water splitting: using CoMoOS/CF or $MoO_2/MoS_2/CoS_2$ mixture as both cathode and anode in 1.0 M KOH. (**b**) Chronopoteniometric curve of CoMoOS catalyst (2.4 mg on CF) as both cathode and anode for overall water splitting at a current density of 10 mA·cm^{-2} for 24 h electrolysis. (**c**) Potential needed to achieve 10 mA·cm^{-2} by different catalysts according to the recent literature: CoMoOS **(1)**, Ni-P/NF **(2)**, [64] $SrNb_{0.1}Co_{0.7}Fe_{0.2}O_{3-\delta}$ perovskite nanorods **(3)**,[65] Ni–P NA/NF **(4)**, [66] FeP nanotubes **(5)**,[67] CoP-rGO **(6)**, [68] $Ni_2P/MoO_2@MoS_2$ **(7)**,[23] N, P co-doped stainless-steel (**8**),[69] Co_2B **(9)** [70] , and Co_xPO_4/CoP **(10)**. [71] (**d**) Generation of bubbles on electrodes during water splitting.

Conclusions

Ultrathin CoS_2-MoS_2 nanoflakes decorated MoO_2 microwires were successfully prepared via partial sulfuration. The obtained CoMoOS showed a high HER performance which is ascribed to synergistic effects among MoO_2, CoS_2-MoS_2, high ECSA (double-layer capacitance 46.3 mF·cm^{-2}) derived from its hierarchical structure as well as its low charge transfer resistance. The catalyst also shows a high OER performance and could be assembled into an alkaline electrolyser for water splitting with a low potential of 1.68 V in alkaline solutions. The synergistic hybridization of nano-flaked MoS_2 and CoS_2 with MoO_2 provides insight into the design and fabrication of promising hierarchical structures for hydrogen evolution in alkaline media.

Conflicts of interest

There are no conflicts to declare.

Acknowledgements

This work is supported by the Australian Research Council through Discovery and Future Fellowship grants (Project No. DP160104089, FT140101256/Selomulya). The help of Thomas Gengenbach (Commonwealth Scientific and Industrial Research Organisation Manufacturing, Clayton, Australia) in performing XPS analysis is gratefully acknowledged. We also acknowledge the use of facilities with the Monash Centre for Electron Microscopy and ARC Funding (LE110100223). We thank the staff, especially Xi-Ya Fang, Emily Chen, and Russell King at the Monash Centre for Electron Microscopy for their assistance with SEM and TEM characterization, respectively. We appreciate the help for XRD characterization and analysis from Jisheng Ma at the Monash X-ray platform. We also thank Yitian Meng and Jun Lu for help in measuring the BET surface area.

Notes and references

1. I. Roger, M. A. Shipman and M. D. Symes, *Nature Reviews Chemistry*, 2017, 1, 0003.
2. X. Zou and Y. Zhang, *Chemical Society Reviews*, 2015, 44, 5148-5180.
3. J. Tian, Q. Liu, A. M. Asiri and X. Sun, *Journal of the American Chemical Society*, 2014, 136, 7587-7590.
4. H. Jin, C. Guo, X. Liu, J. Liu, A. Vasileff, Y. Jiao, Y. Zheng and S.-Z. Qiao, *Chemical Reviews*, 2018, 118, 6337-6408.
5. Y. Wang, B. Kong, D. Zhao, H. Wang and C. Selomulya, *Nano Today*, 2017, 15, 26-55.
6. L. G. Bloor, P. I. Molina, M. D. Symes and L. Cronin, *Journal of the American Chemical Society*, 2014, 136, 3304-3311.
7. L. Han, P. Tang, Á. Reyes-Carmona, B. Rodríguez-García, M. Torréns, J. R. Morante, J. Arbiol and J. R. Galan-Mascaros, *Journal of the American Chemical Society*, 2016, 138, 16037-16045.
8. C. C. L. McCrory, S. Jung, I. M. Ferrer, S. M. Chatman, J. C. Peters and T. F. Jaramillo, *Journal of the American Chemical Society*, 2015, 137, 4347-4357.
9. M.-I. Jamesh and X. Sun, *Journal of Power Sources*, 2018, 400, 31-68.
10. J. Nai, Y. Lu, L. Yu, X. Wang and X. W. Lou, *Advanced Materials*, 2017, 29, 1703870.
11. X. Wang, L. Yu, B. Y. Guan, S. Song and X. W. Lou, *Advanced Materials*, 2018, 30, 1801211.
12. Y. Gou, Q. Liu, X. Shi, A. M. Asiri, J. Hu and X. Sun, *Chemical Communications*, 2018, 54, 5066-5069.
13. L. Ji, Z. Wang, H. Wang, X. Shi, A. M. Asiri and X. Sun, *ACS Sustainable Chemistry & Engineering*, 2018, 6, 4481-4485.
14. L. He, D. Zhou, Y. Lin, R. Ge, X. Hou, X. Sun and C. Zheng, *ACS Catalysis*, 2018, 8, 3859-3864.
15. C. Deng, K.-H. Wu, J. Scott, S. Zhu, R. Amal and D.-W. Wang, *ChemElectroChem*, 2018, 5, 732-736.
16. W. Shao, Y. Xia, X. Luo, L. Bai, J. Zhang, G. Sun, C. Xie, X. Zhang, W. Yan and Y. Xie, *Nano Energy*, 2018, 50, 717-722.
17. J. Xie, J. Xin, R. Wang, X. Zhang, F. Lei, H. Qu, P. Hao, G. Cui, B. Tang and Y. Xie, *Nano Energy*, 2018, 53, 74-82.
18. D. Strmcnik, P. P. Lopes, B. Genorio, V. R. Stamenkovic and N. M. Markovic, *Nano Energy*, DOI: http://dx.doi.org/10.1016/j.nanoen.2016.04.017.
19. Y. Zheng, Y. Jiao, A. Vasileff and S.-Z. Qiao, *Angewandte Chemie International Edition*, 2018, 57, 7568-7579.
20. M. Gong, D.-Y. Wang, C.-C. Chen, B.-J. Hwang and H. Dai, *Nano Research*, 2016, 9, 28-46.

21. X. Lu, X. Tan, D.-W. Wang, Y. H. Ng, H. A. Tahini, H. Tan, W. Yan, S. C. Smith and R. Amal, *Advanced Sustainable Systems*, 2017, 1, 1700032.
22. E. Hu, Y. Feng, J. Nai, D. Zhao, Y. Hu and X. W. Lou, *Energy & Environmental Science*, 2018, 11, 872-880.
23. Y. Wang, T. Williams, T. Gengenbach, B. Kong, D. Zhao, H. Wang and C. Selomulya, *Nanoscale*, 2017, 9, 17349-17356.
24. Y. Liu, C. Xiao, P. Huang, M. Cheng and Y. Xie, *Chem*, 2018, 4, 1263-1283.
25. Y. Ji, L. Yang, X. Ren, G. Cui, X. Xiong and X. Sun, *ACS Sustainable Chemistry & Engineering*, 2018, 6, 11186-11189.
26. D. Liu, C. Zhang, Y. Yu, Y. Shi, Y. Yu, Z. Niu and B. Zhang, *Nano Research*, 2018, 11, 603-613.
27. Y. Huang, X. Chong, C. Liu, Y. Liang and B. Zhang, *Angewandte Chemie International Edition*, 0.
28. C. Zhang, Y. Shi, Y. Yu, Y. Du and B. Zhang, *ACS Catalysis*, 2018, 8, 8077-8083.
29. T. An, Y. Wang, J. Tang, W. Wei, X. Cui, A. M. Alenizi, L. Zhang and G. Zheng, *Journal of Materials Chemistry A*, 2016, 4, 13439-13443.
30. M. S. Faber, M. A. Lukowski, Q. Ding, N. S. Kaiser and S. Jin, *The Journal of Physical Chemistry C*, 2014, 118, 21347-21356.
31. D.-Y. Wang, M. Gong, H.-L. Chou, C.-J. Pan, H.-A. Chen, Y. Wu, M.-C. Lin, M. Guan, J. Yang, C.-W. Chen, Y.-L. Wang, B.-J. Hwang, C.-C. Chen and H. Dai, *Journal of the American Chemical Society*, 2015, 137, 1587-1592.
32. N. Jiang, Q. Tang, M. Sheng, B. You, D.-e. Jiang and Y. Sun, *Catalysis Science & Technology*, 2016, 6, 1077-1084.
33. C. Yang, M. Y. Gao, Q. B. Zhang, J. R. Zeng, X. T. Li and A. P. Abbott, *Nano Energy*, 2017, 36, 85-94.
34. X. Zhao, X. Ma, Q. Lu, Q. Li, C. Han, Z. Xing and X. Yang, *Electrochimica Acta*, 2017, 249, 72-78.
35. J. Zhang, T. Wang, D. Pohl, B. Rellinghaus, R. Dong, S. Liu, X. Zhuang and X. Feng, *Angewandte Chemie*, 2016, 128, 6814-6819.
36. J. Hu, C. Zhang, L. Jiang, H. Lin, Y. An, D. Zhou, M. K. H. Leung and S. Yang, *Joule*, 2017, 1, 383-393.
37. Y. Zhu, J. Dai, W. Zhou, Y. Zhong, H. Wang and Z. Shao, *Journal of Materials Chemistry A*, 2018, 6, 13582-13587.
38. X. Xu, Y. Chen, W. Zhou, Z. Zhu, C. Su, M. Liu and Z. Shao, *Advanced Materials*, 2016, 28, 6442-6448.
39. R. Subbaraman, D. Tripkovic, D. Strmcnik, K.-C. Chang, M. Uchimura, A. P. Paulikas, V. Stamenkovic and N. M. Markovic, *Science*, 2011, 334, 1256-1260.
40. M. Gao, L. Chen, Z. Zhang, X. Sun and S. Zhang, *Journal of Materials Chemistry A*, 2018, 6, 833-836.
41. P. Wang, K. Jiang, G. Wang, J. Yao and X. Huang, *Angewandte Chemie International Edition*, 2016, 55, 12859-12863.
42. J.-X. Feng, H. Xu, Y.-T. Dong, X.-F. Lu, Y.-X. Tong and G.-R. Li, *Angewandte Chemie International Edition*, 2017, 56, 2960-2964.
43. X. Li, P. F. Liu, L. Zhang, M. Y. Zu, Y. X. Yang and H. G. Yang, *Chemical Communications*, 2016, 52, 10566-10569.
44. C. Dong, X. Liu, X. Wang, X. Yuan, Z. Xu, W. Dong, M. S. Riaz, G. Li and F. Huang, *Journal of Materials Chemistry A*, 2017, 5, 24767-24774.
45. H. Yin, S. Zhao, K. Zhao, A. Muqsit, H. Tang, L. Chang, H. Zhao, Y. Gao and Z. Tang, *Nature Communications*, 2015, 6, 6430.
46. Z. Xing, C. Han, D. Wang, Q. Li and X. Yang, *ACS Catalysis*, 2017, 7, 7131-7135.
47. T. Zhang, K. Yang, C. Wang, S. Li, Q. Zhang, X. Chang, J. Li, S. Li, S. Jia, J. Wang and L. Fu, *Advanced Energy Materials*, 0, 1801690.
48. Y. Jin, H. Wang, J. Li, X. Yue, Y. Han, P. K. Shen and Y. Cui, *Advanced Materials*, 2016, 28, 3785-3790.
49. Y. Li, J. Yin, L. An, M. Lu, K. Sun, Y.-Q. Zhao, D. Gao, F. Cheng and P. Xi, *Small*, 2018, 14, 1801070.
50. P. Wang, X. Zhang, J. Zhang, S. Wan, S. Guo, G. Lu, J. Yao and X. Huang, *Nature Communications*, 2017, 8, 14580.
51. Z. Weng, W. Liu, L.-C. Yin, R. Fang, M. Li, E. I. Altman, Q. Fan, F. Li, H.-M. Cheng and H. Wang, *Nano Letters*, 2015, 15, 7704-7710.
52. Z. Chen, K. Leng, X. Zhao, S. Malkhandi, W. Tang, B. Tian, L. Dong, L. Zheng, M. Lin, B. S. Yeo and K. P. Loh, *Nature Communications*, 2017, 8, 14548.
53. L. X. Chen, Z. W. Chen, Y. Wang, C. C. Yang and Q. Jiang, *ACS Catalysis*, 2018, DOI: 10.1021/acscatal.8b01164, 8107-8114.
54. N. Liu, Y. Guo, X. Yang, H. Lin, L. Yang, Z. Shi, Z. Zhong, S. Wang, Y. Tang and Q. Gao, *ACS Applied Materials & Interfaces*, 2015, 7, 23741-23749.
55. L. Chen, J. Zhang, X. Ren, R. Ge, W. Teng, X. Sun and X. Li, *Nanoscale*, 2017, 9, 16632-16637.
56. Y.-F. Xu, M.-R. Gao, Y.-R. Zheng, J. Jiang and S.-H. Yu, *Angewandte Chemie International Edition*, 2013, 52, 8546-8550.
57. N. Danilovic, R. Subbaraman, D. Strmcnik, K.-C. Chang, A. P. Paulikas, V. R. Stamenkovic and N. M. Markovic, *Angewandte Chemie*, 2012, 124, 12663-12666.
58. R. D. Nikam, A.-Y. Lu, P. A. Sonawane, U. R. Kumar, K. Yadav, L.-J. Li and Y.-T. Chen, *ACS Applied Materials & Interfaces*, 2015, 7, 23328-23335.
59. J. Huang, D. Hou, Y. Zhou, W. Zhou, G. Li, Z. Tang, L. Li and S. Chen, *Journal of Materials Chemistry A*, 2015, 3, 22886-22891.
60. H. Zhang, Y. Li, T. Xu, J. Wang, Z. Huo, P. Wan and X. Sun, *Journal of Materials Chemistry A*, 2015, 3, 15020-15023.
61. V. Ganesan, S. Lim and J. Kim, *Chemistry – An Asian Journal*, 2018, 13, 413-420.
62. C. G. Morales-Guio, L. Liardet and X. Hu, *Journal of the American Chemical Society*, 2016, 138, 8946-8957.
63. Z. Huang, Z. Chen, Z. Chen, C. Lv, M. G. Humphrey and C. Zhang, *Nano Energy*, 2014, 9, 373-382.
64. C. Tang, A. M. Asiri, Y. Luo and X. Sun, *ChemNanoMat*, 2015, 1, 558-561.
65. Y. Zhu, W. Zhou, Y. Zhong, Y. Bu, X. Chen, Q. Zhong, M. Liu and Z. Shao, *Advanced Energy Materials*, 2017, 7, 1602122.
66. J. Xiao, Q. Lv, Y. Zhang, Z. Zhang and S. Wang, *RSC Advances*, 2016, 6, 107859-107864.
67. Y. Yan, B. Y. Xia, X. Ge, Z. Liu, A. Fisher and X. Wang, *Chemistry – A European Journal*, 2015, 21, 18062-18067.
68. L. Jiao, Y.-X. Zhou and H.-L. Jiang, *Chemical Science*, 2016, 7, 1690-1695.
69. M.-S. Balogun, W. Qiu, Y. Huang, H. Yang, R. Xu, W. Zhao, G.-R. Li, H. Ji and Y. Tong, *Advanced Materials*, 2017, 29, 1702095.

View Article Online
DOI: 10.1039/C8NR08418A

70. J. Masa, P. Weide, D. Peeters, I. Sinev, W. Xia, Z. Sun, C. Somsen, M. Muhler and W. Schuhmann, *Advanced Energy Materials*, 2016, 6, 1502313.
71. Y. Yang, H. Fei, G. Ruan and J. M. Tour, *Advanced Materials*, 2015, 27, 3175-3180.